NeuroImage 187 (2019) 145–153

Contents lists available at ScienceDirect

NeuroImage

journal homepage: www.elsevier.com/locate/neuroimage

Calibrated fMRI for mapping absolute $CMRO_2$: Practicalities and prospects

M. Germuska, R.G. Wise *

Cardiff University Brain Research Imaging Centre, School of Psychology, Cardiff University, Maindy Road, CF24 4HQ, Cardiff, UK

ARTICLE INFO

Keywords:
BOLD
fMRI
$CMRO_2$
OEF
Oxygen metabolism
Oxygen extraction
Calibrated-fMRI
ASL
Arterial spin labelling
Hypercapnia
Hyperoxia

ABSTRACT

Functional magnetic resonance imaging (fMRI) is an essential workhorse of modern neuroscience, providing valuable insight into the functional organisation of the brain. The physiological mechanisms underlying the blood oxygenation level dependent (BOLD) effect are complex and preclude a straightforward interpretation of the signal. However, by employing appropriate calibration of the BOLD signal, quantitative measurements can be made of important physiological parameters including the absolute rate of cerebral metabolic oxygen consumption or oxygen metabolism ($CMRO_2$) and oxygen extraction (OEF). The ability to map such fundamental parameters has the potential to greatly expand the utility of fMRI and to broaden its scope of application in clinical research and clinical practice. In this review article we discuss some of the practical issues related to the calibrated-fMRI approach to the measurement of $CMRO_2$. We give an overview of the necessary precautions to ensure high quality data acquisition, and explore some of the pitfalls and challenges that must be considered as it is applied and interpreted in a widening array of diseases and research questions.

Introduction

The brain relies predominantly on oxidative metabolism of glucose to satisfy its energy needs in the form of ATP supply (Verweij et al., 2007). Because the brain lacks any fuel reserves it requires a continuous supply of glucose and oxygen. Any disruption of this supply can significantly reduce the production of ATP and negatively affect brain health, with irreversible damage to brain tissue occurring within three minutes of cessation of blood flow (Safar, 1988). Understanding the diseases and mechanisms that can affect oxygen metabolism is of vital importance. The development of widely applicable methods that can measure the cerebral rate of oxygen metabolism ($CMRO_2$) is, therefore, invaluable for the study of metabolic dysfunction.

Over the last few years there have been a number of different MRI approaches proposed to make measurements related to oxygen metabolism, both globally (Jain et al., 2010; Lu and Ge, 2008; Xu et al., 2009) and at the tissue level (Bolar et al., 2011; Fan et al., 2015; Guo and Wong, 2012; He and Yablonskiy, 2007). In this review we focus our discussion on the calibrated fMRI methodology (Bulte et al., 2012; Gauthier et al., 2012; Gauthier and Hoge, 2013; Wise et al., 2013), which shows the potential to map oxygen metabolism at high spatial resolution and with a good level of sensitivity. Although still undergoing development as a technique, the methodology is currently being applied in a number of different diseases and results have been published in Alzheimer's disease (Lajoie et al., 2017a), carotid artery occlusion (De Vis et al., 2015), and in a pharmacological modulation study using caffeine (Merola et al., 2017b). These initial studies have revealed regional changes in $CMRO_2$ that may provide useful insight into the progression of a disease, or action of a drug. This level of detail is clearly one of the key advantages of a tissue based approach, compared to a global measure, and has potential long-term clinical value in a wide range of conditions. The application of this methodology in disease brings new opportunities for understanding brain physiology, but also requires careful consideration of data acquisition, analysis and interpretation. Some disease states may violate fundamental assumptions of the model(s) applied to estimate the physiological parameters, whereas other problems may be overcome with appropriate data acquisition or modification of the analysis. Here we explore the practical issues around data collection, analysis and interpretation with a view to providing guidance as the method is employed in more diverse cohorts of subjects.

Physiological modelling

The basis of dual-calibrated fMRI (dcfMRI), alternatively referred to as quantitative O_2 imaging (Gauthier et al., 2012), is the modulation of blood flow, blood volume, and venous oxygenation during MR imaging via hypercapnic and hyperoxic gas challenges. Physiological models are used to calculate quantitative estimates of the absolute rate of cerebral

* Corresponding author.
E-mail address: wiserg@cardiff.ac.uk (R.G. Wise).

https://doi.org/10.1016/j.neuroimage.2018.03.068
Received 2 October 2017; Received in revised form 14 March 2018; Accepted 28 March 2018
Available online 29 March 2018

metabolic oxygen consumption or oxygen metabolism ($CMRO_2$) from the acquired data. The validity of these estimates is based upon a number of modelling simplifications and physiological assumptions. It is important to consider how these assumptions relate to the underlying physiology and the circumstances under which these assumptions hold when applying the technique. Fig. 1 shows a schematic of the vasculature and how the measured data relate to the underlying physiology.

$CMRO_2$ is linked to the vascular physiology by a complex interplay of physiological parameters. Under the assumption of passive diffusion of oxygen from the capillaries into the tissue, the rate of metabolism is dependent on the rate and pattern of blood flow through the capillaries, the capillary blood volume and its permeability to oxygen, the (arterial) oxygen content of blood entering the capillaries (CaO_2), and the oxygen content in the tissue (CtO_2) (Buxton and Frank, 1997; Jespersen and Ostergaard, 2012; Mintun et al., 2001; Vafaee and Gjedde, 2000; Valabregue et al., 2003). However, the majority of these parameters are not directly accessible via MR imaging methods and inference on the rate of metabolism is instead made using the Fick principle (Fick, 1870). The Fick principle relies on the conservation of mass, and states that the rate of metabolism can simply be determined via equation (1). Thus, in order to calculate a quantitative estimate of resting $CMRO_2$ it is only necessary to measure baseline CBF, OEF and CaO_2. Resting CBF can be calculated from well-established arterial spin labelling (ASL) methods, while the resting OEF is extracted by analysing the modulated ASL and BOLD signals acquired during the dual-calibrated experiment.

$$CMRO_2 = CBF \cdot OEF \cdot CaO_2 \quad (1)$$

The ASL signal is sensitive to the transfer of labelled spins into the extravascular space through the arterioles and capillaries. By choosing an appropriate delay between tagging of the blood and imaging, it is expected that the intravascular contribution from the arterial blood volume (CBV_a) is minimal and that the ASL signal is considered to be purely perfusion weighted (Buxton et al., 1998). During a hypercapnic stimulus perfusion is increased, with the magnitude of this increase (in relation to the change in end-tidal CO_2) being quantified by the cerebral vascular reactivity (CVR). For a hypercapnic stimulus CVR is principally determined by the dilatory response of the arteries and arterioles to the stimulus, i.e. an increase in CBV_a (Kety and Schmidt, 1948; Reivich, 1964). However, the BOLD signal is principally sensitive to changes in CBV_v and CBV_{cap} rather than CBV_a (Ogawa et al., 1993). Therefore, when modelling the BOLD response to hypercapnia we need to estimate blood volume changes in the post-arteriolar vasculature. For simplicity, these two compartments are generally grouped together as one deoxyhaemoglobin sensitive blood volume (CBV in Fig. 1), which is a weighted sum of the capillary and venous compartments (dependent on their respective gradient-echo signal sensitivities and blood volumes). Although there is significant evidence of a variable and an active capillary dilation during functional hyperaemia (Itoh and Suzuki, 2012), current models assume that the blood volume response to hypercapnia is passive in the post-arteriolar network. Thus, ΔCBV is assumed to be proportional to ΔCBV_a and is inferred from a simple power-law model of flow coupling to total blood volume (Grubb et al., 1974) (see equation (2)).

$$\frac{CBV}{CBV_0} = \left(\frac{CBF}{CBF_0}\right)^{\alpha} \quad (2)$$

where α is the 'Grubb exponent', and the subscript '0' denotes the baseline state.

Of course, the BOLD signal is not just sensitive to the blood volume response to hypercapnia but also to the blood flow response via a change in the venous deoxyhaemoglobin content. To model the effect of an increase in perfusion on the BOLD signal it is important to know the metabolic response of the stimulus. Most researchers have assumed that the levels of hypercapnia used in calibrated fMRI are iso-metabolic, namely, blood flow is thought to increase without any alteration in metabolism (Chen and Pike, 2010a). Following the Fick principle of conservation of mass, the OEF must reduce in proportion to the CBF increase in order to maintain the baseline $CMRO_2$. If the arterial deoxyhaemoglobin concentration $[dHb]_a$ is small then the venous deoxyhaemoglobin concentration $[dHb]_v$ is proportional to OEF, and the inverse of the fractional change $[dHb]_v$ is proportional to the change in

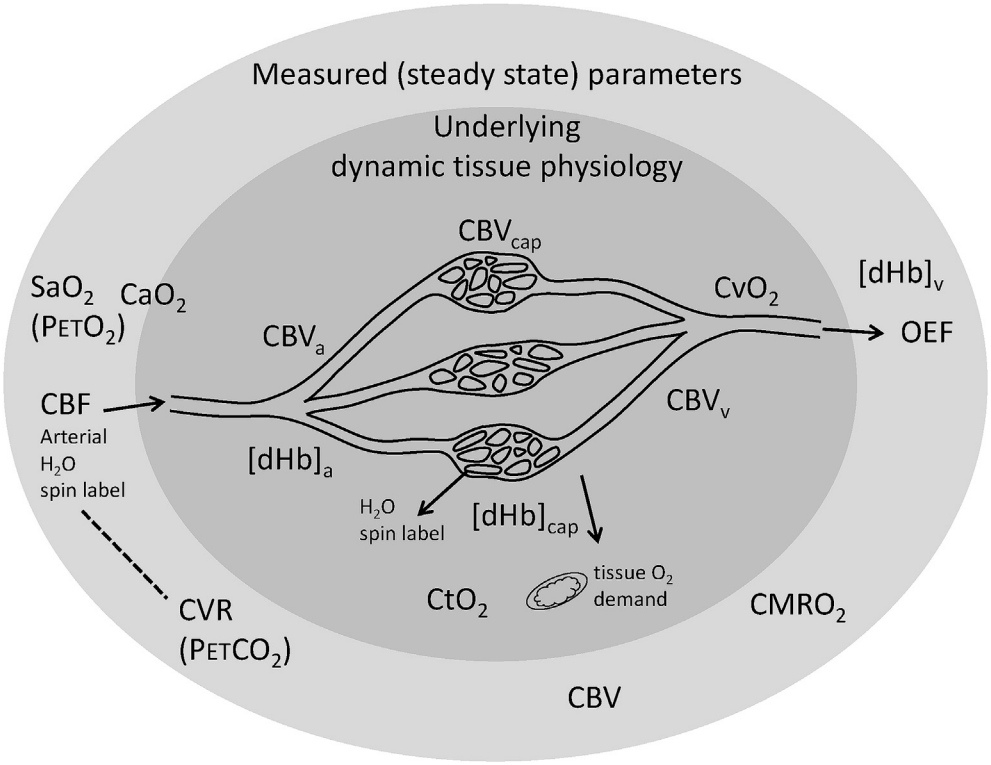

Fig. 1. Cerebral vascular schematic showing the relationship between parameters that are measured or estimated (outer ellipse), by the experimental methods under consideration, and the underlying tissue physiology (inner ellipse) that is not measured or estimated. Arterial oxygen saturation (SaO_2) and arterial oxygen content (CaO_2) may be calculated from the partial pressure of end-tidal oxygen ($P_{ET}O_2$). Cerebral blood flow (CBF) is measured using arterial spin labelling in which the magnetic label is applied to the water in arteries and then interrogated once it diffuses into the tissue compartment (spin label). Cerebrovascular reactivity (CVR) is derived from changes in CBF in response to changes in the partial pressure of end-tidal carbon dioxide ($P_{ET}CO_2$). Cerebral blood volume (CBV), cerebral metabolic rate of oxygen consumption ($CMRO_2$) and oxygen extraction fraction (OEF) are key parameters that are estimated. Compartmental properties include the arterial, capillary and venous blood volumes ($CBV_{a,cap,v}$), arterial, capillary and venous deoxyhaemoglobin concentrations ($[dHB]_{a,cap,v}$), venous oxygen content (CvO_2) and tissue oxygen content (CtO_2).

flow (Hoge et al., 1999) (see equation (3)). While not explicit in the modelling, the change in the BOLD signal will also be dependent on the change in $[dHb]_{cap}$, which has been included in detailed BOLD signal models that have been used for model validation (Merola et al., 2016).

$$\frac{CBF}{CBF_0} = \frac{[dHb]_{v0}}{[dHb]_v} \tag{3}$$

Hyperoxic stimuli are considered in a similar manner to hypercapnic flow changes, in that they are treated as an iso-metabolic increase in oxygen availability (Chiarelli et al., 2007). If CBF is fixed while arterial oxygen content CaO_2 is increased (by increased haemoglobin carried oxygen and oxygen dissolved in blood plasma), then via the Fick principle OEF must also be fixed to maintain baseline $CMRO_2$. Thus, at steady state with fixed CBF, the arteriovenous O_2 difference ($CaO_2 - CvO_2$) must equal the baseline value. Therefore, for any hyperoxic increase in CaO_2 there will be an equivalent change in CvO_2, from which the change in $[dHb]_v$ can be estimated. In reality, increases in arterial oxygen saturation (SaO_2) are known to alter CBF. It is likely that this is principally a result of an associated reduction arterial partial pressure of CO_2 ($PaCO_2$) (Iscoe and Fisher, 2005), as animal studies demonstrate that when $PaCO_2$ is fixed hyperoxia has no effect on CBF (Asher et al., 1988). Equation (4) (Wise et al., 2013) links arbitrary changes in CBF and CaO_2 to the BOLD signal; it incorporates CaO_2 changes during CBF modulation and vice-versa. It is perhaps interesting to note that increases in CaO_2 result in an approximately linear decrease in $[dHb]_v$ that is mostly independent of its resting value, while changes in CBF result in a fractional change in $[dHb]_v$. This fundamental difference between the two stimuli is what enables us to factor out resting $[dHb]_v$, and thus OEF, when analysing data from both physiological interventions.

$$\frac{\Delta S}{S_0} = M\left\{1 - \left(\frac{CBF}{CBF_0}\right)^{\alpha}\left(\frac{[dHb]_v}{[dHb]_{v0}}\right)^{\beta}\right\} \tag{4a}$$

$$\frac{[dHb]_v}{[dHb]_{v0}} = \frac{CBF_0}{CBF} - \frac{1}{[dHb]_{v0}}\left\{\frac{1}{\phi}\left(CaO_2 - \left(\frac{CBF_0}{CBF}\right)CaO_{2,0}\right) + [Hb]\left(\frac{CBF_0}{CBF} - 1\right)\right\} \tag{4b}$$

β is a field strength dependent term relating the BOLD signal to underlying vascular morphology and water diffusion, M is a calibration parameter representing a maximal BOLD response, φ is the O_2 carrying capacity of haemoglobin (1.34 ml O_2/g_{Hb}), [Hb] is the haemoglobin concentration in the BOLD sensitive vasculature, $SvO_{2,0}$ is the percentage of oxygen bound to haemoglobin in the venous vasculature at baseline, $[dHb]_{vo} = [Hb](1\text{-}SvO_{2,0})$, and $OEF = (CaO_2 - CvO_2)/CaO_2$.

Applications of the method

The first published application of dcfMRI in neurodegenerative disease investigates the regional variation in oxygen metabolism in Alzheimer's disease (AD) (Lajoie et al., 2017a), which is known to be associated with alterations in $CMRO_2$ (Buckner et al., 2005). Consistent with earlier PET studies (Frackowiak et al., 1981; Fukuyama et al., 1994; Ishii et al., 1996; Tohgi et al., 1998) dcfMRI revealed a significantly reduced $CMRO_2$ in the parietal lobe compared to controls. However, no correlation was found between the imaging parameters and the cognitive assessment scores (Montreal Cognitive Assessment). This study also highlighted an important dependence on arterial transit time for the accurate assessment of $CMRO_2$ via dcfMRI. Regions with long transit times (e.g. occipital lobe) were shown to underestimate resting CBF and overestimate the change in CBF with hypercapnia. As a result, OEF and $CMRO_2$ estimates in the occipital lobe were shown to be underestimated in both controls and AD patients.

A (more) rapid acquisition protocol, which consisted of 6.5 min of respiratory modulation, was used in the assessment of vascular disease in internal carotid artery occlusion (De Vis et al., 2015). This pilot study sought to assess the ability of the method to detect variances in cerebral haemodynamics associated with the disease. However, the results showed no significant differences in CBF, OEF or $CMRO_2$ between patients and controls, and a large variance in all measured parameters. Again, due to the sensitivity of the ASL signal to transit time effects, the issue of delayed transit time is a probable confound for the assessment of $CMRO_2$ in vascular occlusion and other large vessel diseases. The authors note that use of velocity selective ASL (VSASL) could overcome these issues due to its inherent insensitivity to arterial transit time. Although conventional VSASL has a significantly reduced CNR compared to other tagging methods, more recent developments of the technique demonstrate superior GM SNR compared to conventional tagging approaches with moderate delay times (Guo and Wong, 2015).

The use of dcfMRI in pharmacological studies has been investigated using caffeine in a cohort of healthy volunteers (Merola et al., 2017b). This study aimed to investigate the global (grey matter) and regional sensitivity of the method to simultaneous alterations in CBF and OEF. The results demonstrated a significant GM decrease in CBF and increase in OEF, with regional decreases in $CMRO_2$. These reductions in $CMRO_2$ are consistent with previous PET-FDG results (Park et al., 2014), although are at odds with some MRI studies, which have shown both increases (Griffeth et al., 2011) and no change (Xu et al., 2015) in $CMRO_2$ with caffeine. The data presented by Merola, Xu, and Griffeth all used similar doses of caffeine, 200–250 mg. The observed increase in global OEF reported by Xu et al. is similar to that reported by Merola et al., 18.6% versus the 16%. However, the global CBF reduction (16.4%) reported by Xu et al. is significantly less than the 30% grey matter reduction observed by Merola et al. and the 27% reduction observed by Griffeth et al. Thus, the results of the proof-of-principle study from Merola et al. present a view of a regional variation of $CMRO_2$ where the changes in CBF and OEF are consistent with alternative acquisition methods. However, we would highlight the need for further comprehensive validation studies using these new methods.

Sensitivity to physiological assumptions

Due to the reliance on hypercapnic and hyperoxia gas challenges many of the assumptions that influence a conventional calibrated bold experiment also affect the dual-calibrated approach, (see (Hoge, 2012) for a review). Here we discuss the detail of the principal confounds from the perspective of the dual-calibrated approach. As previously noted there is the fundamental requirement in calibrated BOLD experiments that the hypercapnic and hyperoxic stimuli do not alter oxygen metabolism. Meeting these conditions means that the ASL signal and the arterial oxygen content can be used to infer the $[dHb]_v$ changes caused by the stimuli. A number of studies (Chen and Pike, 2010a; Xu et al., 2011) have investigated the validity of this fundamental assumption in healthy volunteers and while there is conflicting evidence regarding the effect of mild hypercapnia on oxygen metabolism, any changes is metabolism are generally assumed to be small for the stimuli used in calibrated fMRI experiments. However, any changes in metabolism during hypercapnia or hyperoxia can have a significant influence on OEF (and thus $CMRO_2$ estimates); see simulations in (Merola et al., 2016).

When using calibrated methods to investigate drugs or disease there are a number of physiological conditions under which significant changes in metabolism are possible or even likely. For example, where oxygen metabolism is suppressed due to limited oxygen delivery any increase in CBF or CaO_2 is likely to be coupled with an increase in metabolism, e.g. in stroke or other diseases where metabolism is restricted due to reduced perfusion. Additionally, many of the conditions that we would like to study may suffer from hypo-metabolism due to limited oxygen supply, rather than mitochondrial dysfunction (where we may not expect alterations in metabolism due to increased supply). The oxygen supply may be restricted either by limited perfusion, restricted diffusion of oxygen into the tissue, or a combination of both. It is unclear exactly how these restrictions to oxygen delivery and the metabolic rate

of oxygen consumption will interact with hypercapnic and hyperoxic stimuli, thus care must clearly be taken as this new methodology is exploited to investigate metabolic dysfunction.

The flow-volume relationship described by equation (2) is based on empirical data measured in animal studies (Grubb et al., 1974) and later re-produced in human volunteers (Chen and Pike, 2010b). Its use in the model and analysis generally assumes a fixed and uniform functional relationship between CBF and venous volume changes. However, to the best of our knowledge this relationship has not been studied in disease or altered states of physiology where such assumptions may no longer hold. Indeed, the flow-volume relationship could vary across healthy tissue, change with alterations in baseline conditions (e.g. if a subject has increased/reduced perfusion pressure), or be affected by focal disease. This shortfall has been well recognized by the imaging community and proposals have been made to map volume-flow coupling during a dcfMRI experiment (Wise et al., 2013). However, as demonstrated by Merola et al. (2016) the co-linearity in the models between α and another vascular parameter, 'β', (which relates the BOLD signal to the vascular morphology) means that these parameters are not separable by the proposed implementation. Alternative methods have also been proposed to measure the vascular morphology during a dcfMRI examination (Germuska and Bulte, 2014), where vessel size imaging information is simultaneously acquired with the addition of a spin-echo readout. Incorporation of such information could resolve the co-linearity problem and allow direct estimation of α. However, vessel size data is inherently noisy and such an experiment would require careful optimization of the acquisition protocol to avoid the propagation of noise in the analysis.

The assumption of a fixed flow-volume relationship could potentially create even greater issues as the method is implemented at higher resolution, as is now practicable with the increased availability of ultra high field scanners. As the resolution is increased the assumption that ASL perfusion changes are co-localised with BOLD sensitive CBV changes may not hold. This is particularly relevant if attempting to map $CMRO_2$ through the cortical layers, where significant CBF changes may no longer occur in the same voxels as the relevant BOLD CBV changes, and thus the effective alpha may change significantly between voxels and across layers. Furthermore, careful consideration needs to be given to the fundamental assumption of the conservation of mass used in the derivation of the BOLD equations. If the measured CBF changes are no longer co-localised with the associated venous oxygenation changes then this assumption is no longer valid and the Fick relationships underpinning the method are not relevant.

A common assumption when implementing these methods is that a systemic measure of haemoglobin concentration [Hb] at or near the time of examination is a reliable estimate of the cerebral [Hb] in the venous vasculature. While this is likely to be a good approximation at rest, and minimal differences in the closely related parameter, haematocrit (Hct), have been found across grey matter in healthy volunteers, there is evidence showing significant regional changes in Hct during disease progression (Loutfi et al., 1987) and (Okazawa et al., 1996). The change in Hct, and therefore [Hb], appears to be due to a change in the plasma concentration of the blood, which may be compensated for by an increase in OEF (Okazawa et al., 1996). The plasma concentration (and blood velocity) is also the principal driver for the difference between large and small vessel Hct via the Fahraeus effect (Gaehtgens, 1981). Thus, regional differences in Hct can also be expected due to variation in small vessel volume (which may also be altered dynamically via vasodilation). Without correction for these effects, such changes in haemoglobin concentration would be misinterpreted as a change in $CMRO_2$. A potential MRI method to map resting cerebral Hct has been proposed (Calamante et al., 2016) that requires the additional acquisition of a dynamic susceptibility contrast DSC-MRI dataset (whose parameter estimates are Hct weighted). While such additional data acquisitions could limit the applicability of the technique, it may be necessary in certain disease states and may offer additional scope to extend the modelling and analysis of the calibrated data.

Blood gas modulation for calibration

Here we describe the practical set-up for the manipulation of end-tidal gases and present different approaches for gas manipulation and data collection when performing dcfMRI (Fig. 2, Tables 1 and 2). There are two fundamental approaches to modulating end-tidal gases, fixed inspired fractions and targeted end-tidal changes. End-tidal targeting may either be prospective (Ito et al., 2008) or dynamic (Wise et al., 2007), that is, gas changes can be pre-calculated (depending on individual physiology) or updated in real-time (or a combination of the two). The simplest form of dynamic end-tidal targeting employs manual control of flow meters to adjust gas delivery relying on skilled experimenters to adjust the inspirate. However, automated methods have also been proposed (Wise et al., 2007). Dynamic adjustment of gas delivery requires a short sampling lag, which necessitates a short sampling line between the subject and gas monitor. Due to the restrictions of the MR environment this can be difficult to achieve and particularly in the case of automated methods can lead to instability in end-tidal traces. However, newer commercial systems are becoming available that seek to address

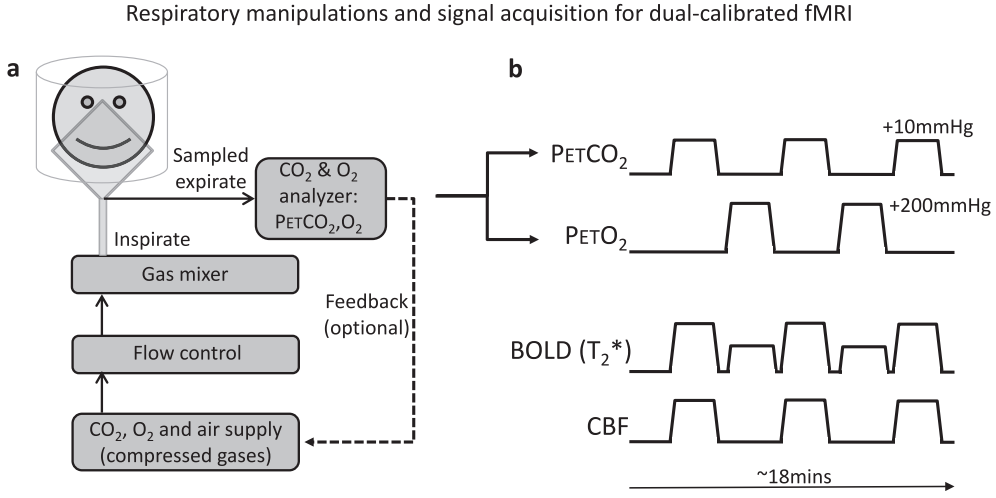

Fig. 2. Schematic of respiratory manipulations needed for calibrated fMRI (a and b) and the corresponding idealised BOLD and CBF time-courses (b). Typical experimental duration and respiratory manipulations are indicated. See also Table 1 for a description of respiratory manipulations and Table 2 for a description of MR acquisition strategies.

Table 1
The advantages and disadvantages of different respiratory challenge implementations for the modulation of cerebral blood flow and oxygenation, necessary steps of the calibration of fMRI signals.

Method	Pros	Cons
Fixed inspired challenge (nasal cannula)	Convenient and comfortable, easy to perform, low cost.	Risk of poor end-tidal control and measurement. Slower transitions.
Fixed inspired challenge (with face mask)	Easy to perform, low cost. Can be made more consistent with automated control.	Face mask less convenient. End-tidal values not targeted - depend on ventilatory response, slower transitions.
Prospective end-tidal targeting (with face mask)	Complex end-tidal waveforms achievable. Can be performed by automated/expert manual control. Fast transitions.	Expensive and complex control system required for automated control. Lack of feedback may result in drift of end-tidal values.
Feedback-based dynamic end tidal targeting (with face mask)	Complex end-tidal waveforms achievable. Can be performed by automated/expert manual control. Fast transitions.	Expensive and complex control system required for automated control. Feedback sensitive to sampling delays.

Table 2
The advantages and disadvantages of different schemes for MR signal acquisition in dual-calibrated fMRI for the assessment of OEF and $CMRO_2$.

Method	Pros	Cons
Single echo ASL	Widely available, shortest TR, shortest total ASL volume readout (good coverage)	Compromised (non optimal) BOLD and ASL contrast to noise; background suppression would compromise BOLD.
Dual echo ASL	Optimal ASL signal (especially with short TE spiral readout) and BOLD contrast from the later echo	Less widely available; longer volume readout (e.g. reducing ASL signal in superior slices); background suppression would compromise BOLD.
Dual Excitation ASL (alternate ASL, BOLD volumes, minimizing TR)	Optimal ASL signal especially with background suppression, short ASL volume readout (good coverage), good BOLD CNR.	Longer TR; ASL and BOLD not acquired simultaneously, BOLD CNR slightly compromised by BG suppression/short BOLD TR.

this issue by employing an MR compatible gas analyser in the scan room. In the interest of simplicity, and to avoid some of the issues associated with end-tidal targeting, a more straightforward approach is to simply deliver pre-defined concentrations of gases. Again, this may either be achieved manually or under computer-automated control.

In principle, the accurate targeting of end-tidal CO_2 ($P_{ET}CO_2$) or O_2 ($P_{ET}O_2$) is the preferred method. As discussed in the modelling section, the change in venous oxygen concentration (CvO_2) due to an oxygen challenge is directly related to the change in CaO_2, and thus PaO_2. If the alveolar-arterial oxygen tension difference is small, as is expected in the absence of compromised gas exchange function of the lungs, then $P_{ET}O_2$ is a reliable estimate of PaO_2 (Bengtsson et al., 2001). Therefore, targeted modulation of $P_{ET}O_2$ in fact allows for a controlled and repeatable modulation of CvO_2. By similar reasoning, because CBF is monotonically related to steady-state $PaCO_2$ (Shapiro et al., 1966), targeted increases in $P_{ET}CO_2$, allow for controlled and repeatable increases in CBF (with the magnitude of change in CBF determined by the local CVR). Additionally, a well-controlled experiment that uses end-tidal targeting can allow for the modulation of one gas while clamping the level of another, e.g. modulation of O_2 while holding end-tidal CO_2 constant. This is a potentially useful function that can simplify the analysis somewhat and may help to increase the reliability of experiments. Fig. 2a shows a schematic of the experimental set-up for a calibrated fMRI scan, while Table 1 summarises the advantages and trade-offs associated with each gas manipulation method.

For a typical fixed inspired experiment, an interleaved paradigm is used with an inspired oxygen fraction (FiO_2) of 50% and an inspired CO_2 fraction of 5%. The choice of FiO_2 is determined by a trade-off between maximising the BOLD response in hyperoxia and avoiding significant artefacts from paramagnetic molecular O_2 in the airways and sinuses, T_1-shortening effects that may affect CBF quantification, and any potential alteration in metabolism. However, there is still debate about the appropriate level and whether greater inspired fractions are a practical alternative (Lajoie et al., 2017b). The choice of 5% for the CO_2 challenge is mainly dictated by patient comfort and the need for an iso-metabolic challenge. A 5% CO_2 stimulus is well tolerated by the majority of subjects both in our experience and more generally (Lajoie et al., 2016). However, we would advise that any CO_2 challenge be trialled on naive subjects outside of the scan environment, allowing them to become accustomed to the sensation of elevated $PaCO_2$ prior to any scan session. In our experience typical end-tidal gas changes for such fixed inspiration experiments range from approximately 200-300 mmHg for the O_2 stimulus and approximately 8–12 mmHg for the CO_2 stimulus, depending on the participant's ventilatory response. When using targeted gas delivery, values that lie in the centre of these ranges are typically chosen. Mapping of CVR performed with a CO_2 stimulus is an associated method that has been performed safely in hundreds of patients and volunteers. In 2013 a review of the safety and tolerability of CVR scanning performed in 434 CVR examinations (294 patients) was published (Spano et al., 2013). In all cases a targeted end-tidal change of 10 mmHg was prescribed (from 40 mmHg at baseline up to 50 mmHg during hypercapnia). The protocol included 45 s and 130 s blocks of hypercapnia interleaved around a 90 s baseline, age range of participants 9–88 years old (mean 45.9 years $\pm$ 20.6). Transient symptoms during the hypercapnic phase were reported in 11.1% of patients, these symptoms included shortness of breath, headache, and dizziness; fewer than 6% of all subjects withdrew due to such symptoms. There were no lasting effects due to the intervention and no major complications. Systematic evaluations of tolerability for dcfMRI protocols have not yet been undertaken, however, the determining factor is likely to be the level and duration of hypercapnic stimuli used during the examination, and reported findings of tolerability agree well with the experience of CVR examinations. Using a fixed inspiration protocol (5% CO_2 and 50% O_2) dcfMRI was performed in 34 Alzheimer's patients (mean age 76.9 years $\pm$ 6.5) and 37 controls (mean age 74.4 $\pm$ 4.6) (Lajoie et al., 2017a). During hypercapnic testing 10% of controls and 17% of patients withdrew. As highlighted in their manuscript, the elevated dropout rate for controls is probably associated with increase age of the participants, whereas the greater dropout rate for AD patients may be associated with the disease.

Some of the principle concerns when delivering gas mixtures to a participant are to ensure there is low resistance in the breathing circuit, sufficient supply to match peak inspiration, minimal dead space (to reduce re-breathing of expirate) and accurate monitoring of end-tidal gases. Additionally, it is important to consider the failure mode of the circuit, i.e. what will the subject breath if there is an interruption in the gas supply. There are different ways to address these concerns, with more options available when end-tidal values are not being controlled (as this requires tight control of inspired fractions, Table 1). The most straightforward method to deliver and record gases is the use of a dual nasal cannula, which allows the delivery of gas to both nostrils while simultaneously sampling the expirate. This method is inherently low resistance, has no dead space and is capable of providing accurate monitoring of end-tidal gases. However, each breath of inspired gas will be a mixture of room air and that delivered by the cannula, limiting the maximum deliverable concentrations. Additionally, practical experience shows that it is easy for the placement of the cannula to move during an experiment,

restricting delivery and potentially providing inaccurate monitoring of end-tidal gases. A common alternative is to use an MRI compatible mask with an appropriate breathing circuit. If the breathing circuit is properly designed, a well performing and reliable system is achievable using off the shelf components. One such breathing circuit has been proposed by Tancredi et al. (2014). The circuit uses a combination of valves to provide a minimal dead space and a small reservoir to meet peak inspiratory requirements, while simultaneously allowing breathing of room air in the failure mode. With the addition of low resistance filters on the gas inlet and sample outlet, this circuit forms the basis of the breathing system we use for the majority of our current gas modulation studies.

In addition to the delivery method, the experimental design or gas paradigm, can have a significant effect on the quality and interpretability of the experiment. The simplest paradigm, and probably most utilized so far, is the interleaved design. With this method periods of baseline (air) are interleaved with O_2 and CO_2 block challenges (Fig. 2b), sometimes with pre/de-emphasis added to the O_2 blocks to speed transition from baseline to stable hyperoxia (Germuska et al., 2016). Modelling studies, based upon dual-echo PASL data, suggest that the error in $CMRO_2$ estimates is minimised with approximately equal time spent in each state, that is baseline, hyperoxia, and hypercapnia (Germuska et al., 2014). While the optimal gas paradigm is likely to change depending on end-tidal targets, FiO_2, $FiCO_2$, and acquisition scheme (e.g. PASL, pCASL, background suppression, single echo readout, or dual-echo readout, Fig. 2b and Table 2) this equally weighted paradigm is likely to be a robust design for most approaches. An alternative to the interleaved design is the simultaneous design, where O_2 and CO_2 end-tidal values are modulated at the same time. The principle advantage of this approach is the possibility to encode more physiological data into the experiment. While the interleaved design is essentially composed of two experiments (an O_2 challenge and a CO_2 challenge) the simultaneous design can be thought of as multiple experiments, with each experiment consisting of different levels of O_2 and CO_2 modulation. The extra information provided by these paradigms can potentially be used to aid in fitting of the data (Gauthier et al., 2012) or to extract extra parameters from the data (Wise et al., 2013). However, when using a simultaneous gas paradigm it is necessary to consider any potential contrast-to-noise (CNR) ratio sacrifices that are made, e.g. if using O_2 or CO_2 challenges that are less than the maximum allowable.

MRI data acquisition and analysis

Fig. 2b depicts idealised respiratory traces and expected MR signals for an interleaved dcfMRI experiment. As shown in the diagram, it is necessary to simultaneously acquire both CBF and BOLD weighted data in order to solve for the resting $CMRO_2$. Here we identify and compare (Table 2) three principle methods of data acquisition, single-echo ASL (Bulte et al., 2012), dual/multi-echo ASL (Gauthier et al., 2012; Germuska and Bulte, 2014; Wise et al., 2013), and dual-excitation ASL. In each of these methods the ASL data can be acquired either using a pulsed (PASL), continuous, or more often, pseudo-continuous (pCASL) tagging scheme. As in any ASL acquisition, the CNR advantages of pCASL acquisition schemes offer a significant advantage over PASL methods. However, due to systemic alteration in CBF caused by hypercapnia, the effect of inversion efficiency changes may pose a greater challenge in the analysis of calibrated fMRI than in conventional acquisitions.

The most straightforward data acquisition method is to use a single-echo readout as employed in a traditional ASL scanning. However, the echo time is increased to somewhere in the region of 20 ms to increase the BOLD weighting. This method has the clear advantage of easy implementation and acquires the BOLD and CBF data simultaneously. However, the CNR of both the ASL and BOLD data is limited due to a compromise in echo times that is sub-optimal for both ASL and BOLD acquisitions. Additionally, application of background suppression (which can significantly increase ASL CNR) is likely to significantly reduce the BOLD CNR, and so to the best of our knowledge has not been employed for single-echo readouts. To overcome the compromise of choosing a single echo time a number of studies have employed a dual-echo readout, where a second BOLD-weighted echo is readout immediately following the ASL readout. The advantage of this acquisition scheme is that an optimal echo time can be chosen for each echo, creating a predominately CBF-weighted echo and a predominately BOLD-weighted echo. The main disadvantage of this approach compared to the single-echo readout is the increased readout time per slice. This increase in readout time means that for the same number of slices there will be a significant increase in the spread of post labelling delay times from inferior to superior slices (assuming bottom up acquisition of the data). This increase in the range of post labelling delay times will manifest either as an increase in arterial contamination (in inferior slices) or as a reduction in CNR (in superior slices), or a combination of the two. The application of background suppression will again have a significant negative influence on the BOLD CNR. However, because of the increased BOLD-weighting it may be possible to include a moderate amount of background suppression and still retain sufficient BOLD CNR. The final acquisition method currently used to acquire dcfMRI data is the dual-excitation acquisition scheme. This acquisition scheme essentially employs interleaved ASL and BOLD acquisitions. After each ASL tagging/control period a volume of CBF-weighted data is acquired (as in a conventional ASL scan), which is then quickly followed by the acquisition of a BOLD-weighted volume. The acquisition scheme is less temporally efficient than the dual-echo scheme, requiring an extra 100–300ms per TR to acquire the same volume of data. Additionally, there will be approximately 500–1000ms difference between the acquisition time of the CBF-weighted data and BOLD-weighted data (depending on sequence parameters). Despite these limitations, there are a number of advantages of acquiring the data in this manner. Because the readout time per slice is the same as the single-echo readout, the sequence is well suited to full brain coverage, not suffering from the same degree of arterial contamination or reduced CNR in superior slices associated with dual-echo readouts. Furthermore, standard background suppression methods can be employed to greatly increase the CNR of the ASL data without significantly affecting the CNR of the BOLD readout (Schmithorst et al., 2014). In our experience the ability to employ background suppression in a dual-excitation acquisition outweighs the disadvantages of the approach, producing good quality $CMRO_2$ maps across the grey matter. Fig. 3 shows example $CMRO_2$ maps obtained in an individual volunteer using an 18-min dual-excitation pCASL acquisition with background suppression applied as described in (Okell et al., 2013) (TR 4.4 s, TE_{ASL} 10 ms, TE_{BOLD} 30 ms, tagging duration 1.5 s, post-labelling delay 1.5 s, GRAPPA acceleration factor of 3, $3.4 \times 3.4 \times 7$mm voxels, 20% slice gap, 16 slices, respiratory stimulus as described in (Germuska et al., 2016)).

Because the dual-calibrated method is still undergoing development there is yet to be any consensus regarding data analysis. From the point of view of data modelling there are two principle approaches, the separate hypercapnia and hyperoxia method proposed by Bulte et al. (2012) and the combined or generalised calibration method described by Gauthier et al. (Gauthier and Hoge, 2013) and Wise et al. (2013). The method proposed by Bulte et al. has the advantage of being straightforward and easy to implement. However, as previously highlighted (Hoge, 2012), it can result in errors in the estimation of OEF when arterial saturation drops below approximately 95% (due to the implicit assumption of 100% saturation in the models). Additionally, the generalised calibration model(s) allow for the assessment of arbitrary and simultaneous changes in arterial CO_2 and O_2. This is useful for a number of reasons, enabling the analysis of more complex gas modulations (Wise et al., 2013), or for the analysis of the complete acquisition time series (Germuska et al., 2016). When analysing the entire data time series, parameter estimates and end-tidal respiratory traces are fed through the generalised model to obtain a best fit to the acquired data. Although this approach increases the complexity of the analysis, modelling studies and in-vivo acquisitions suggest that such an approach makes better use of the available data and provides more robust estimates of OEF.

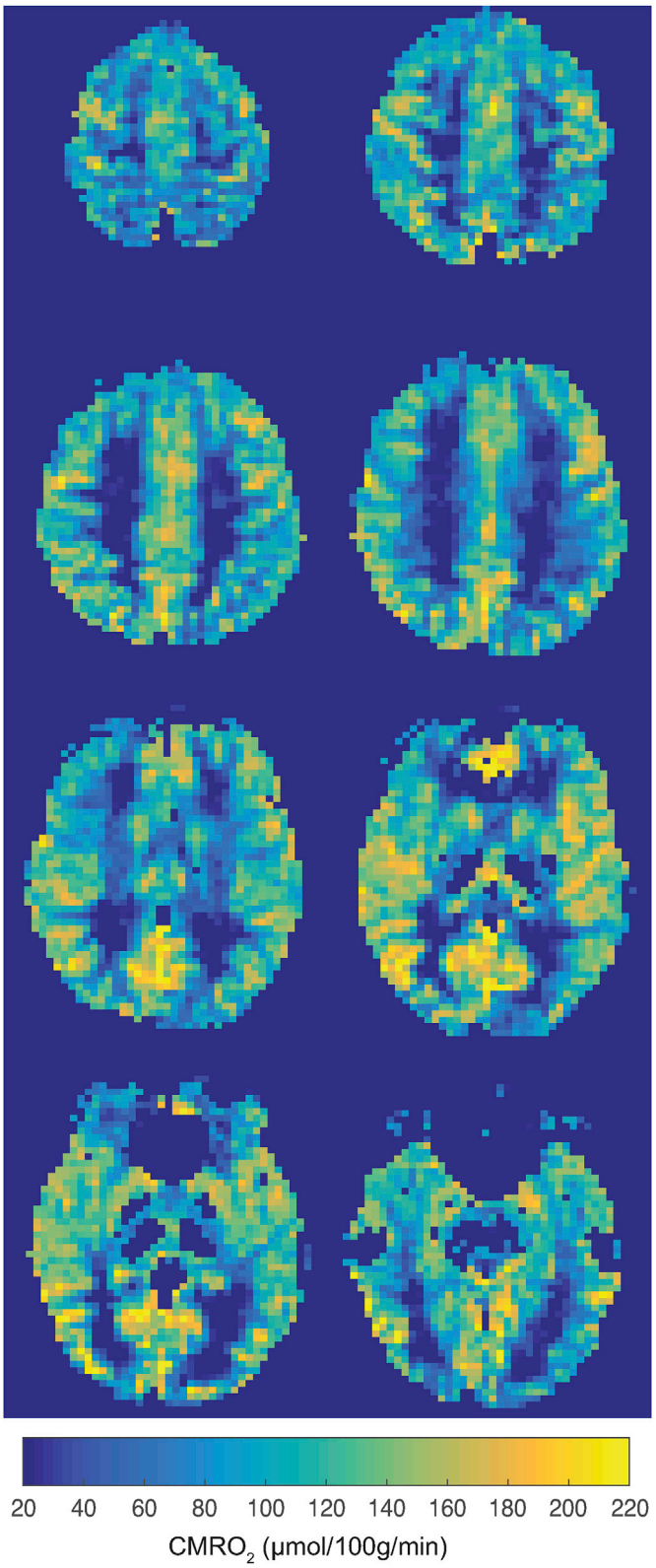

Fig. 3. Example $CMRO_2$ parameter maps acquired from a single subject using a dual-excitation pCASL acquisition with background suppression.

Reliability

As dcfMRI is applied to a wider variety of populations and patient groups it is essential that the repeatability of the method is characterised and taken into consideration when interpreting results of longitudinal studies, performing statistical power calculations, or identifying regional alterations in metabolism. So far data has been presented on the repeatability from two small groups of healthy volunteers (Lajoie et al., 2016), n = 8 and (Merola et al., 2017a) n = 12. The results from these studies show modest repeatability of within subject grey matter (GM) parameters. With Lajoie et al. reporting GM coefficient of variations of 3.9%, 13.6%, and 15.2% for resting CBF, OEF, and $CMRO_2$ respectively. Merola et al. found similar results with GM coefficient of variations of 6.9%, 6.7%, and 12.0% respectively. Additionally, the investigation by Merola found that nearly all subjects had an ICC of greater than 0.6 (generally classified as 'good)' for the voxel-wise correlation of $CMRO_2$ values both within session and across days. The repeatability of GM estimates is somewhat comparable with PET measures of repeatability, which report GM coefficient of variations of 8.8%, 9.3%, and 5.3% (for CBF, OEF, and $CMRO_2$ respectively) (Bremmer et al., 2011) and 4.6%, 2.1%, and 3.7% (Coles et al., 2006). However, the time to acquire the data is significantly shorter, 18 min for MRI data acquisition versus approximately 45 min for the PET acquisitions. Additionally, the dcfMRI methodology removes the need for ionising radiation, arterial blood sampling and the onsite cyclotron necessary to perform a ^{15}O PET examination. The high ICC reported for the voxel-wise analysis is encouraging as it demonstrates good repeatability of voxel-wise estimates on a per subject basis. This is important if the method is to be used to assess regional changes either as a result of disease or due to an intervention.

In addition to the repeatability of the method, the sensitivity and accuracy of the method are key factors in determining its usefulness as a biomarker. A repeatable measure with a high level of sensitivity can be used to identify sub-groups or for the assessment of individual patients rather than just reporting average or group effects, while a high level of accuracy ensures that the parameters are biologically interpretable and can help in our scientific understanding of the condition being studied. Although there have been no comprehensive investigations of the method's sensitivity, the initial findings are encouraging. Investigations in Alzheimer's disease (Lajoie et al., 2017a) demonstrated a significant reduction in OEF within the parietal lobe (voxel-wise analysis), and an investigation on the effects of caffeine (Merola et al., 2017b) found a significant GM increase in OEF with regional reductions in $CMRO_2$. The accuracy of the method has been investigated in a study undertaken by Fan et al. (2016), who compared calibrated measures of OEF against a susceptibility based MR imaging method in eleven healthy volunteers. The data were compared in terms of the agreement between techniques, and in the ability of baseline measurements to predict CBF responses to visual stimulation. The reported data shows reasonable agreement between the two methods ($R^2 = 0.39$) and similar correlations between resting OEF and the visual CBF response, $R^2 = 0.37$ and 0.36 for the calibrated and susceptibility based methods respectively. Additionally, investigations in healthy volunteers (Germuska et al., 2016) showed a strong negative correlation ($R^2 = 0.66$) between resting CBF and OEF, which are comparable with whole brain measures by Lu et al. (2008). Thus, demonstrating the expected coupling between these two parameters and demonstrating the ability of the technique to detect variation in both measured and derived parameters in individual subjects. Although these initial findings are promising, there is still a clear need for further investigation with specific interventions and conditions to provide more quantitative information on the sensitivity and accuracy of the method.

Prospects

The aim of dcfMRI is to offer an alternative method to ^{15}O PET for the quantitative mapping of cerebral oxygen metabolism. In principle dcfMRI offers several advantages including availability, acquisition time, and reduced risk (lack of ionising radiation). Due to the lack of ionising radiation, repeat examinations can be carried out without significant risk to participants, thus this opens the door for longitudinal studies to assess changes in baseline metabolism. This is a significant advantage compared to PET imaging of $CMRO_2$, and we anticipate a significant role for dcfMRI

in this area. Another potential advantage of the technique is its multi-parametric nature, for example it inherently provides extra vascular information in the BOLD and ASL CVR parameters, and provides information on the dHb weighted blood volume via the oxygen gas modulation. Additionally, it is straightforward to incorporate additional MRI contrasts that could be used to tease out further metabolic or vascular information (Germuska and Bulte, 2014), or potentially increase the robustness of the technique.

Over the last 3–4 years a number of groups have already taken up the method and are looking at disease, drug and age related changes in metabolism. Some of the results from these studies show considerable promise for the technique, but they also highlight some of the technical challenges related to the measurement. The principal technical challenge appears to be the robust measurement of CBF. Because the CBF measurement is based on ASL, any restrictions and challenges that apply to ASL also apply to dcfMRI. Therefore, for example, accurate measurement of $CMRO_2$ is challenging in the presence of long arterial transit times. In order to overcome these challenges, ASL free methods of calculating the BOLD calibration parameter M have been proposed (Blockley et al., 2015; Blockley and Stone, 2016). These methods, based on the measurement of basal R_2', remove the need for a CO_2 gas challenge and thus avoid the need to measure small changes in the ASL signal. However, because these methods are based on the resting R_2' value, rather than an oxygenation dependent signal change, they are sensitive to additional sources of susceptibility such as myelin content or iron deposits. This is a significant challenge for such techniques and further developments are required if this confound is to be overcome. Nevertheless, the incorporation of such techniques into the calibrated fMRI framework has the potential to increase the robustness and applicability of the technique, allowing its application in cohorts where a CO_2 gas challenge may be contraindicated or unfeasible. Undoubtedly, through the use of such methods and other developments in data acquisition and analysis such those that we have shown to experimental design and estimation procedures, the calibrated fMRI techniques will continue to improve and will find novel application in the assessment of brain energetics and oxygen metabolism in the coming years.

Acknowledgements

MG and RW acknowledge the generous support of the Wellcome Trust (Wellcome Trust Strategic Award entitled ‘Multi-scale and multi-modal assessment of coupling in the healthy and diseased brain’, grant reference 104943/Z/14/Z). RW thanks the Higher Education Funding Council for Wales (HEFCW) and the UK Engineering and Physical Sciences Research Council (EP/K020404/1) for supporting the development of the calibrated fMRI methods described at CUBRIC.

References

Asher, A.S., Burns, G.P., Luber, J.M., Fox, D., Wise, L., 1988. Effect of increasing inspired oxygen concentration on hemodynamics and regional blood flows. Crit. Care Med. 16, 1235–1237.
Bengtsson, J., Bake, B., Johansson, A., Bengtson, J.P., 2001. End-tidal to arterial oxygen tension difference as an oxygenation index. Acta Anaesthesiol. Scand. 45, 357–363.
Blockley, N.P., Griffeth, V.E., Simon, A.B., Dubowitz, D.J., Buxton, R.B., 2015. Calibrating the BOLD response without administering gases: comparison of hypercapnia calibration with calibration using an asymmetric spin echo. Neuroimage 104, 423–429.
Blockley, N.P., Stone, A.J., 2016. Improving the specificity of R2' to the deoxyhaemoglobin content of brain tissue: prospective correction of macroscopic magnetic field gradients. Neuroimage 135, 253–260.
Bolar, D.S., Rosen, B.R., Sorensen, A.G., Adalsteinsson, E., 2011. QUantitative Imaging of eXtraction of oxygen and TIssue consumption (QUIXOTIC) using venular-targeted velocity-selective spin labeling. Magn. Reson Med. 66, 1550–1562.
Bremmer, J.P., van Berckel, B.N., Persoon, S., Kappelle, L.J., Lammertsma, A.A., Kloet, R., Luurtsema, G., Rijbroek, A., Klijn, C.J., Boellaard, R., 2011. Day-to-day test-retest variability of CBF, CMRO2, and OEF measurements using dynamic 15O PET studies. Mol. Imaging Biol. 13, 759–768.
Buckner, R.L., Snyder, A.Z., Shannon, B.J., LaRossa, G., Sachs, R., Fotenos, A.F., Sheline, Y.I., Klunk, W.E., Mathis, C.A., Morris, J.C., Mintun, M.A., 2005. Molecular, structural, and functional characterization of Alzheimer's disease: evidence for a relationship between default activity, amyloid, and memory. J. Neurosci. 25, 7709–7717.
Bulte, D.P., Kelly, M., Germuska, M., Xie, J., Chappell, M.A., Okell, T.W., Bright, M.G., Jezzard, P., 2012. Quantitative measurement of cerebral physiology using respiratory-calibrated MRI. Neuroimage 60, 582–591.
Buxton, R.B., Frank, L.R., 1997. A model for the coupling between cerebral blood flow and oxygen metabolism during neural stimulation. J. Cereb. Blood Flow. Metab. 17, 64–72.
Buxton, R.B., Frank, L.R., Wong, E.C., Siewert, B., Warach, S., Edelman, R.R., 1998. A general kinetic model for quantitative perfusion imaging with arterial spin labeling. Magn. Reson Med. 40, 383–396.
Calamante, F., Ahlgren, A., van Osch, M.J., Knutsson, L., 2016. A novel approach to measure local cerebral haematocrit using MRI. J. Cereb. Blood Flow. Metab. 36, 768–780.
Chen, J.J., Pike, G.B., 2010a. Global cerebral oxidative metabolism during hypercapnia and hypocapnia in humans: implications for BOLD fMRI. J. Cereb. Blood Flow. Metab. 30, 1094–1099.
Chen, J.J., Pike, G.B., 2010b. MRI measurement of the BOLD-specific flow-volume relationship during hypercapnia and hypocapnia in humans. Neuroimage 53, 383–391.
Chiarelli, P.A., Bulte, D.P., Wise, R., Gallichan, D., Jezzard, P., 2007. A calibration method for quantitative BOLD fMRI based on hyperoxia. Neuroimage 37, 808–820.
Coles, J.P., Fryer, T.D., Bradley, P.G., Nortje, J., Smielewski, P., Rice, K., Clark, J.C., Pickard, J.D., Menon, D.K., 2006. Intersubject variability and reproducibility of 15O PET studies. J. Cereb. Blood Flow. Metab. 26, 48–57.
De Vis, J.B., Petersen, E.T., Bhogal, A., Hartkamp, N.S., Klijn, C.J., Kappelle, L.J., Hendrikse, J., 2015. Calibrated MRI to evaluate cerebral hemodynamics in patients with an internal carotid artery occlusion. J. Cereb. Blood Flow. Metab. 35, 1015–1023.
Fan, A.P., Govindarajan, S.T., Kinkel, R.P., Madigan, N.K., Nielsen, A.S., Benner, T., Tinelli, E., Rosen, B.R., Adalsteinsson, E., Mainero, C., 2015. Quantitative oxygen extraction fraction from 7-Tesla MRI phase: reproducibility and application in multiple sclerosis. J. Cereb. Blood Flow. Metab. 35, 131–139.
Fan, A.P., Schafer, A., Huber, L., Lampe, L., von Smuda, S., Moller, H.E., Villringer, A., Gauthier, C.J., 2016. Baseline oxygenation in the brain: correlation between respiratory-calibration and susceptibility methods. Neuroimage 125, 920–931.
Fick, A., 1870. Uber die Messung des Blutquantums in den Herzventrikeln. Seitung Phys. Med. Ges. Würzbg. 2, 290–291.
Frackowiak, R.S., Pozzilli, C., Legg, N.J., Du Boulay, G.H., Marshall, J., Lenzi, G.L., Jones, T., 1981. Regional cerebral oxygen supply and utilization in dementia. A clinical and physiological study with oxygen-15 and positron tomography. Brain 104, 753–778.
Fukuyama, H., Ogawa, M., Yamauchi, H., Yamaguchi, S., Kimura, J., Yonekura, Y., Konishi, J., 1994. Altered cerebral energy metabolism in Alzheimer's disease: a PET study. J. Nucl. Med. 35, 1–6.
Gaehtgens, P., 1981. Distribution of flow and red cell flux in the microcirculation. Scand. J. Clin. Lab. Invest. Suppl. 156, 83–87.
Gauthier, C.J., Desjardins-Crepeau, L., Madjar, C., Bherer, L., Hoge, R.D., 2012. Absolute quantification of resting oxygen metabolism and metabolic reactivity during functional activation using QUO2 MRI. Neuroimage 63, 1353–1363.
Gauthier, C.J., Hoge, R.D., 2013. A generalized procedure for calibrated MRI incorporating hyperoxia and hypercapnia. Hum. Brain Mapp. 34, 1053–1069.
Germuska, M., Bulte, D.P., 2014. MRI measurement of oxygen extraction fraction, mean vessel size and cerebral blood volume using serial hyperoxia and hypercapnia. Neuroimage 92, 132–142.
Germuska, M., Merola, A., Murphy, K., Babic, A., Richmond, L., Khot, S., Hall, J.E., Wise, R.G., 2016. A forward modelling approach for the estimation of oxygen extraction fraction by calibrated fMRI. Neuroimage 139, 313–323.
Germuska, M., Merola, A., Murphy, K., Wise, R.G., 2014. An optimised respiratory paradigm for the Bayesian estimation of OEF by calibrated MRI. Imaging Cereb. Physiol. Leipz. Meet. Manip. Magn. Reson. contrast through Respir. Chall.
Griffeth, V.E., Perthen, J.E., Buxton, R.B., 2011. Prospects for quantitative fMRI: investigating the effects of caffeine on baseline oxygen metabolism and the response to a visual stimulus in humans. Neuroimage 57, 809–816.
Grubb Jr., R.L., Raichle, M.E., Eichling, J.O., Ter-Pogossian, M.M., 1974. The effects of changes in PaCO2 on cerebral blood volume, blood flow, and vascular mean transit time. Stroke 5, 630–639.
Guo, J., Wong, E.C., 2012. Venous oxygenation mapping using velocity-selective excitation and arterial nulling. Magn. Reson Med. 68, 1458–1471.
Guo, J., Wong, E.C., 2015. Increased SNR efficiency in velocity selective arterial spin labeling using multiple velocity selective saturation modules (mm-VSASL). Magn. Reson Med. 74, 694–705.
He, X., Yablonskiy, D.A., 2007. Quantitative BOLD: mapping of human cerebral deoxygenated blood volume and oxygen extraction fraction: default state. Magn. Reson Med. 57, 115–126.
Hoge, R.D., 2012. Calibrated FMRI. Neuroimage 62, 930–937.
Hoge, R.D., Atkinson, J., Gill, B., Crelier, G.R., Marrett, S., Pike, G.B., 1999. Investigation of BOLD signal dependence on cerebral blood flow and oxygen consumption: the deoxyhemoglobin dilution model. Magn. Reson Med. 42, 849–863.
Iscoe, S., Fisher, J.A., 2005. Hyperoxia-induced hypocapnia: an underappreciated risk. Chest 128, 430–433.
Ishii, K., Kitagaki, H., Kono, M., Mori, E., 1996. Decreased medial temporal oxygen metabolism in Alzheimer's disease shown by PET. J. Nucl. Med. 37, 1159–1165.
Ito, S., Mardimae, A., Han, J., Duffin, J., Wells, G., Fedorko, L., Minkovich, L., Katznelson, R., Meineri, M., Arenovich, T., Kessler, C., Fisher, J.A., 2008. Non-

invasive prospective targeting of arterial P(CO2) in subjects at rest. J. Physiol. 586, 3675–3682.
Itoh, Y., Suzuki, N., 2012. Control of brain capillary blood flow. J. Cereb. Blood Flow. Metab. 32, 1167–1176.
Jain, V., Langham, M.C., Wehrli, F.W., 2010. MRI estimation of global brain oxygen consumption rate. J. Cereb. Blood Flow. Metab. 30, 1598–1607.
Jespersen, S.N., Ostergaard, L., 2012. The roles of cerebral blood flow, capillary transit time heterogeneity, and oxygen tension in brain oxygenation and metabolism. J. Cereb. Blood Flow. Metab. 32, 264–277.
Kety, S.S., Schmidt, C.F., 1948. The effects of altered arterial tensions of carbon dioxide and oxygen on cerebral blood flow and cerebral oxygen consumption of normal young men. J. Clin. Invest. 27, 484–492.
Lajoie, I., Nugent, S., Debacker, C., Dyson, K., Tancredi, F.B., Badhwar, A., Belleville, S., Deschaintre, Y., Bellec, P., Doyon, J., Bocti, C., Gauthier, S., Arnold, D., Kergoat, M.J., Chertkow, H., Monchi, O., Hoge, R.D., 2017a. Application of calibrated fMRI in Alzheimer's disease. Neuroimage Clin. 15, 348–358.
Lajoie, I., Tancredi, F.B., Hoge, R.D., 2016. Regional reproducibility of bold calibration parameter M, OEF and resting-state CMRO2 measurements with QUO2 MRI. PLoS One 11 e0163071.
Lajoie, I., Tancredi, F.B., Hoge, R.D., 2017b. The impact of inspired oxygen levels on calibrated fMRI measurements of M, OEF and resting CMRO2 using combined hypercapnia and hyperoxia. PLoS One 12 e0174932.
Loutfi, I., Frackowiak, R.S., Myers, M.J., Lavender, J.P., 1987. Regional brain hematocrit in stroke by single photon emission computed tomography imaging. Am. J. Physiol. Imaging 2, 10–16.
Lu, H., Ge, Y., 2008. Quantitative evaluation of oxygenation in venous vessels using T2-Relaxation-Under-Spin-Tagging MRI. Magn. Reson Med. 60, 357–363.
Lu, H., Zhao, C., Ge, Y., Lewis-Amezcua, K., 2008. Baseline blood oxygenation modulates response amplitude: physiologic basis for intersubject variations in functional MRI signals. Magn. Reson Med. 60, 364–372.
Merola, A., Germuska, M., Murphy, K., Wise, R.G., 2017a. Assessing the repeatability of absolute CMRO2 measurements from calibrated fMRI. In: ISMRM 25th Annual Meeting Honolulu, HI. USA.
Merola, A., Germuska, M.A., Warnert, E.A., Richmond, L., Helme, D., Khot, S., Murphy, K., Rogers, P.J., Hall, J.E., Wise, R.G., 2017b. Mapping the pharmacological modulation of brain oxygen metabolism: the effects of caffeine on absolute CMRO2 measured using dual calibrated fMRI. Neuroimage 155, 331–343.
Merola, A., Murphy, K., Stone, A.J., Germuska, M.A., Griffeth, V.E.M., Blockley, N.P., Buxton, R.B., Wise, R.G., 2016. Measurement of oxygen extraction fraction (OEF): an optimized BOLD signal model for use with hypercapnic and hyperoxic calibration. Neuroimage 129, 159–174.
Mintun, M.A., Lundstrom, B.N., Snyder, A.Z., Vlassenko, A.G., Shulman, G.L., Raichle, M.E., 2001. Blood flow and oxygen delivery to human brain during functional activity: theoretical modeling and experimental data. Proc. Natl. Acad. Sci. U. S. A. 98, 6859–6864.
Ogawa, S., Menon, R.S., Tank, D.W., Kim, S.G., Merkle, H., Ellermann, J.M., Ugurbil, K., 1993. Functional brain mapping by blood oxygenation level-dependent contrast magnetic resonance imaging. A comparison of signal characteristics with a biophysical model. Biophys. J. 64, 803–812.
Okazawa, H., Yonekura, Y., Fujibayashi, Y., Yamauchi, H., Ishizu, K., Nishizawa, S., Magata, Y., Tamaki, N., Fukuyama, H., Yokoyama, A., Konishi, J., 1996. Measurement of regional cerebral plasma pool and hematocrit with copper-62-labeled HSA-DTS. J. Nucl. Med. 37, 1080–1085.
Okell, T.W., Chappell, M.A., Kelly, M.E., Jezzard, P., 2013. Cerebral blood flow quantification using vessel-encoded arterial spin labeling. J. Cereb. Blood Flow. Metab. 33, 1716–1724.
Park, C.A., Kang, C.K., Son, Y.D., Choi, E.J., Kim, S.H., Oh, S.T., Kim, Y.B., Park, C.W., Cho, Z.H., 2014. The effects of caffeine ingestion on cortical areas: functional imaging study. Magn. Reson Imaging 32, 366–371.
Reivich, M., 1964. Arterial Pco2 and cerebral hemodynamics. Am. J. Physiol. 206, 25–35.
Safar, P., 1988. Resuscitation from clinical death: pathophysiologic limits and therapeutic potentials. Crit. Care Med. 16, 923–941.
Schmithorst, V.J., Hernandez-Garcia, L., Vannest, J., Rajagopal, A., Lee, G., Holland, S.K., 2014. Optimized simultaneous ASL and BOLD functional imaging of the whole brain. J. Magn. Reson Imaging 39, 1104–1117.
Shapiro, W., Wasserman, A.J., Patterson Jr., J.L., 1966. Mechanism and pattern of human cerebrovascular regulation after rapid changes in blood CO2 tension. J. Clin. Invest. 45, 913–922.
Spano, V.R., Mandell, D.M., Poublanc, J., Sam, K., Battisti-Charbonney, A., Pucci, O., Han, J.S., Crawley, A.P., Fisher, J.A., Mikulis, D.J., 2013. CO2 blood oxygen level-dependent MR mapping of cerebrovascular reserve in a clinical population: safety, tolerability, and technical feasibility. Radiology 266, 592–598.
Tancredi, F.B., Lajoie, I., Hoge, R.D., 2014. A simple breathing circuit allowing precise control of inspiratory gases for experimental respiratory manipulations. BMC Res. Notes 7.
Tohgi, H., Yonezawa, H., Takahashi, S., Sato, N., Kato, E., Kudo, M., Hatano, K., Sasaki, T., 1998. Cerebral blood flow and oxygen metabolism in senile dementia of Alzheimer's type and vascular dementia with deep white matter changes. Neuroradiology 40, 131–137.
Vafaee, M.S., Gjedde, A., 2000. Model of blood-brain transfer of oxygen explains nonlinear flow-metabolism coupling during stimulation of visual cortex. J. Cereb. Blood Flow. Metab. 20, 747–754.
Valabregue, R., Aubert, A., Burger, J., Bittoun, J., Costalat, R., 2003. Relation between cerebral blood flow and metabolism explained by a model of oxygen exchange. J. Cereb. Blood Flow. Metab. 23, 536–545.
Verweij, B.H., Amelink, G.J., Muizelaar, J.P., 2007. Current concepts of cerebral oxygen transport and energy metabolism after severe traumatic brain injury. Prog. Brain Res. 161, 111–124.
Wise, R.G., Harris, A.D., Stone, A.J., Murphy, K., 2013. Measurement of OEF and absolute CMRO2: MRI-based methods using interleaved and combined hypercapnia and hyperoxia. Neuroimage 83, 135–147.
Wise, R.G., Pattinson, K.T., Bulte, D.P., Chiarelli, P.A., Mayhew, S.D., Balanos, G.M., O'Connor, D.F., Pragnell, T.R., Robbins, P.A., Tracey, I., Jezzard, P., 2007. Dynamic forcing of end-tidal carbon dioxide and oxygen applied to functional magnetic resonance imaging. J. Cereb. Blood Flow. Metab. 27, 1521–1532.
Xu, F., Ge, Y., Lu, H., 2009. Noninvasive quantification of whole-brain cerebral metabolic rate of oxygen (CMRO2) by MRI. Magn. Reson Med. 62, 141–148.
Xu, F., Liu, P., Pekar, J.J., Lu, H., 2015. Does acute caffeine ingestion alter brain metabolism in young adults? Neuroimage 110, 39–47.
Xu, F., Uh, J., Brier, M.R., Hart Jr., J., Yezhuvath, U.S., Gu, H., Yang, Y., Lu, H., 2011. The influence of carbon dioxide on brain activity and metabolism in conscious humans. J. Cereb. Blood Flow. Metab. 31, 58–67.